A computational study of wetting on chemically contaminated substrates

Tobias Luginsland* and Roger A. Sauer

Aachen Institute for Advanced Study in Computational Engineering Science (AICES), RWTH Aachen University, Templergraben 55, 52056 Aachen, Germany

Published[1] in *Colloids and Surfaces A*, DOI: 10.1016/j.colsurfa.2017.06.031
Submitted on 5 March 2017; Revised on 11 June 2017; Accepted on 12 June 2017

Abstract

The partial wetting of droplets on rigid, chemically contaminated substrates is investigated numerically for Bond numbers $Bo \leq 5$. To this end a recently developed numerical framework (Sauer, 2014; Sauer et al., 2014) based on a finite element discretisation and a computational contact algorithm is used. Its applicability to wetting on chemically heterogeneous substrates is demonstrated. An analytical expression for the change in the apparent contact angle in the presence of an arbitrarily strong chemical contamination is derived based on a perturbed force equilibrium analogy at the triple phase contact line. The analytical prediction is compared to the theory by de Gennes (1985) as well as to the modified Cassie's law (Cassie, 1948) with perfect agreement in the limit of small perturbations, i.e. small chemical contaminations. The predicted change in the apparent contact angle is used to define a mapping between the droplet shape for wetting on homogeneous substrates and chemically heterogeneous substrates. Numerical results are presented for circular, patterned substrates (axial and radial patterns) as well as locally introduced perturbations on otherwise homogeneous substrates. The results for the droplet shape on chemically contaminated substrates show good agreement with the analytical solution for the droplet's height and wetting radius on homogeneous substrates when the presented mapping is applied. Moreover, the present results are in good quantitative agreement to results reported in literature.

Keywords: Wetting, chemical contaminations, numerical methods, contact angle, interface heterogeneity

1 Introduction

The wetting dynamics of droplets on topographically or chemically heterogeneous or contaminated substrates is of importance in nature as well as in a variety of technical applications. The wetting of plant leaves by rain droplets, such as the lotus leaf (Bittoun and Marmur, 2012) or the elephant's ear leaf (Quéré, 2008) is an example from nature, where the substrate's topography significantly influences the wetting process. Paint and ink spreading in printing processes, the use of adhesives in industrial applications and hydrophilic/hydrophobic coatings in the chemical industry are common examples of wetting processes in technical contexts involving droplets on heterogeneous substrates. To understand the differences in the wetting process on heterogeneous substrates compared to homogeneous substrates is therefore of fundamental

*corresponding author, email: luginsland@aices.rwth-aachen.de
[1]This pdf is the personal version of an article whose journal version is available at www.sciencedirect.com

interest. Recently, some progress has been made in the field by means of experiments, theoretical predictions and numerical investigations. Major results can be found in the reviews by Quéré (2008) on wetting of topographically heterogeneous (textured) substrates, by Bonn et al. (2009) on the (thermo-)dynamics of wetting on rough and chemically heterogeneous substrates as well as by Snoeijer and Andreotti (2013) on the dynamics of moving contact lines. The wetting of chemically and/or topographically heterogeneous substrates features some interesting phenomena not observed on perfectly homogeneous substrates, such as anisotropic spreading, inhibition of droplet spreading, discontinuities in the spreading process as well as the observation of more than one equilibrium state for an identical droplet/substrate scenario. In the following we briefly review some contributions to the understanding of wetting on chemically heterogeneous substrates (Sec. 2) and motivate the present investigation (Sec. 3).

2 Literature survey on chemically heterogeneous substrates

In this section we review contributions to the field of wetting on chemically heterogeneous substrates. We focus thereby on studies that investigate the wetting on chemically heterogeneous substrates, where the substrate's wettability properties change at distinct locations, i.e. areas with different properties are separated by clearly identifiable borders. This wetting scenario corresponds to the substrate's surface properties studied in the present investigation, as described in Sec. 3. Furthermore, we mainly restrict ourselves to reviewing numerical studies.

Schwartz and Eley (1997) investigated by means of numerical simulation the dynamic droplet spreading on a chemically heterogeneous substrate. The substrate was thereby composed of two materials with significantly different wetting properties. The authors found that the motion of the droplet is almost discontinuous in the event of a droplet breakup. The breakup process is thereby dominated by wetting forces, and instability mechanisms play a minor role only.

Woodward et al. (2000) studied experimentally the partial wetting characteristics on chemically heterogeneous substrates composed of random hydrophilic and hydrophobic patches with typical length scales in the nanometer regime. They found the measured contact angle for water to be lower than the theoretical prediction by Cassie (1948) and argued that long-range hydrophobic interactions may result in an effective increase of the hydrophobic patch area compared to the hydrophilic one altering the equilibrium contact angle. For the length scales considered, the results were independent of the droplet size indicating line tension effects to be minimal.

Vellingiri et al. (2011) extended the numerical investigations of Savva and Kalliadasis (2009) and Savva et al. (2010) to the spreading of two-dimensional droplets on chemically heterogeneous substrates assuming small contact angles. The chemical heterogeneity was thereby accounted for by local variations in the microscopic contact angle acting as a boundary condition to the governing equations. As for the case of a topographically heterogeneous substrate, multiple equilibria existed for identical droplet/substrate configurations and a stick-slip behavior was observed at the droplet front. The wetting state of droplets on periodically heterogeneous substrates showed a behavior that could not be explained by the Cassie relation (Cassie, 1948), cf. also Woodward et al. (2000).

Buehrle et al. (2002) numerically studied the shape of liquid droplets on substrates with a lateral striped wettability pattern and focused on the wettability contrast, the transition sharpness and the line tension of the triple phase contact line. The results revealed the influence of the local wettability of the substrate, the local curvature of the contact line and the lateral gradients in the line tension on the local contact angle and its modulation. The modulation of the local

contact angle decreased with an increasing contact line tension and with a decreasing sharpness of the wettability pattern.

In the numerical study by Dupuis and Yeomans (2004) the spreading of droplets on striped, chemically heterogeneous substrates was studied by means of Lattice Boltzmann (LB) simulations solving the Navier-Stokes equations. While the spreading on homogeneous substrates revealed a clear functional dependence of the wetting radius on a dimensionless time independent of the surface tensions and viscosities (cf. also Snoeijer and Andreotti (2013)), the wetting velocity was anisotropic for the case of a striped substrate. The equilibrium shape of the sessile droplet was highly influenced by the underlying pattern of the chemically heterogeneous substrate.

Adão et al. (1999) investigated the wetting characteristics of droplets on regularly and randomly distributed chemical heterogeneities by means of Molecular Dynamics (MD) simulations. The size of the heterogeneities was thereby on the atomistic length scale. The authors were able to show the validity of Cassie's law (Cassie, 1948) for equilibrium contact angles in the presence of molecular heterogeneities on the substrate.

In their MD simulations, Lundgren et al. (2007) investigate the behavior of nano-scale droplets on checker board-patterned and striped chemically heterogeneous substrates. The authors found the ratio of the domain size to the initial droplet size to be of importance in such simulations, particularly when the droplet size is comparable to the domain size. Furthermore, they showed that the specific topography—striped, checker-boarded or pillar structured—and composition of the substrate is of importance for the equilibrium wetting state. Depending on the specific properties of the substrate the contact behavior between the droplet and the solid was not well described by the Wenzel (Wenzel, 1936), Cassie (Cassie, 1948) or Cassie and Baxter equations (Cassie and Baxter, 1944) and the quantitative agreement was poor.

Iliev and Pesheva (2003) studied numerically the wetting properties of chemically heterogeneous, circular substrates (axial and radial patterns). The influence of the substrate's heterogeneity on the equilibrium wetting state of the droplet was discussed and the results were analyzed in the light of the applicability of the Cassie or modified Cassie equation (Cassie, 1948). For the first type of heterogeneity the Cassie as well as the modified Cassie equation was valid and the approximation became better when the droplet size increased relative to the length scale of the heterogeneity. For the second pattern the Cassie equation was reasonably well satisfied.

Regarding the validity of the Wenzel (Wenzel, 1936), (modified) Cassie (Cassie, 1948) and Cassie and Baxter equations (Cassie and Baxter, 1944) the majority of authors agree upon droplet size effects as the main reason for the observed deviations from theory. If the droplet size is chosen sufficiently large compared to the length scale of the substrate's heterogeneities, the resulting wetting state is well described by the theoretical predictions.

3 Motivation of the present work

In the present investigation we introduce a new approach for the numerical investigation of chemically contaminated substrates. The new numerical approach is based on the Finite Element Method (FEM) representing sessile droplets as liquid membranes under hydrostatic conditions (Sauer et al., 2014). The chemical contaminations are thereby accounted for via a force equilibrium analogy due to their influence on the surface tension, which in turn affects the triple phase contact line between the partially wetting droplet and the rigid substrate. At the solid-liquid interface a computational contact mechanical algorithm is applied to capture the spreading behavior during the wetting process. The representation of a droplet as a liquid-filled membrane

and the interpretation of chemical heterogeneities from the mechanical point of view as well as the numerical framework based on a contact algorithm and the FEM is new to the scientific community. The new approach is applied to chemically contaminated substrates, where the contamination affects either the entire triple phase contact line or only parts of it.

Some types of chemical contaminations the approach is able to model (but not limited to) are depicted schematically in Fig. 1. Axially and radially patterned substrates are shown in subfigures (a) and (b), the first corresponding to the regime II setup of Lipowsky et al. (1999). An axially-radially patterned substrate is depicted in subfigure (c), where only parts of the triple phase contact line are affected by the change in the substrate's wetting properties. A special case of an axially-radially patterned substrate is shown in subfigure (d), the so-called dartboard pattern. Subfigures (e) and (f) show chemically locally perturbed substrates were either the entire or only parts of the contact line are affected in analogy to de Gennes (1985). In the described scenarios, the differences in the wetting characteristics may either be due to the local properties of the substrate itself or due to a liquid film of infinitely small height coating parts of the substrate's surface.

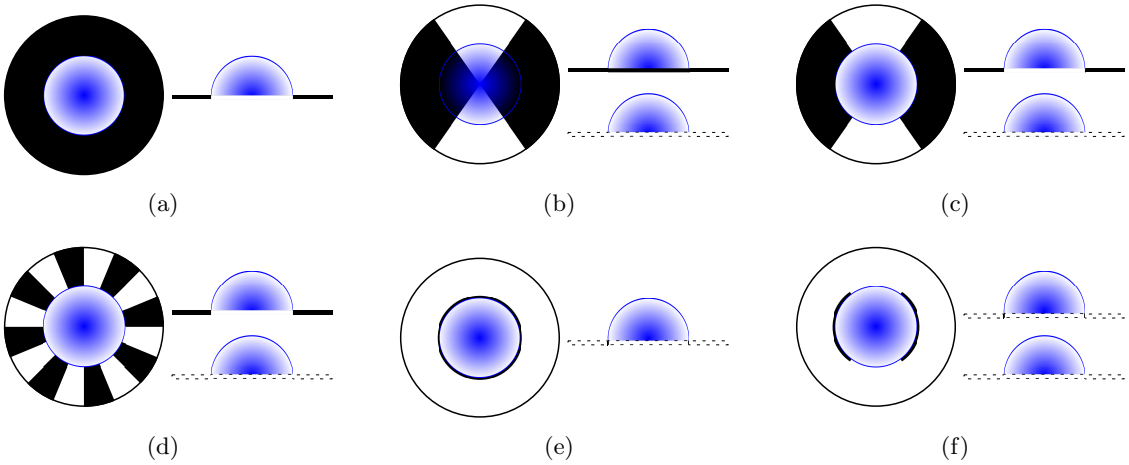

Figure 1: Schematic sketches of the partial wetting scenarios on chemically heterogeneous substrates considered in the present investigation. (a) Axially and (b) radially patterned substrates, (c) Axially-radially patterned substrate, (d) Dartboard patterned substrate. (e+f) Chemically locally perturbed substrates. In each subfigure the top view (left) and side view (right) is depicted with the droplet indicated in blue. The different wetting properties of the substrate are indicated in black and white.

The remainder of this paper is organized as follows. In Sec. 4 the analytical theory by de Gennes (1985) for weak chemical contaminations is recast and a perturbed force equilibrium analogy at the triple phase contact line is presented. It is shown that in the limiting case of small contaminations, the predicted change in the local contact angle is identical for both theories. Additionally, the perturbed force equilibrium analogy is shown to be valid for large contaminations and therefore to be applicable in a more general fashion. Furthermore, the modified Cassie's law (Cassie, 1948) is reformulated in the present context. In Sec. 5 the numerical framework is introduced. In Sec. 6 numerical results are presented and compared to analytical predictions for the Bond number $Bo = 0$ and chemical contaminations affecting the entire triple phase contact line. Furthermore, results are discussed for the presence of gravity ($0 < Bo \leq 5$) and for contaminations acting on parts of the droplet only. In Sec. 7 we summarize our findings and conclude our study, giving some remarks on possible extensions of the present study.

4 Analytical theory

In this section we recast the analytical theory presented by de Gennes (1985) for weakly perturbed substrates in the presence of chemical contaminations and introduce the perturbed force equilibrium analogy governing the force equilibrium at the triple phase contact line for chemically heterogeneous substrates. We show that for the limit of small perturbations the change in the apparent contact angle predicted by the force equilibrium analogy is identical to the theory by de Gennes (1985). Furthermore, we comment on Cassie's law (Cassie, 1948) for chemically heterogeneous substrates and its interpretation in the present context.

4.1 The theory of locally, weakly perturbed substrates by de Gennes (1985)

de Gennes (1985) introduced an analytical theory for the presence of a chemical contamination, or weak fluctuation, on the substrate at the location $\mathbf{x} = (x, y)^{\mathrm{T}}$ (for arbitrary Bond numbers). The chemical contamination $\delta(\mathbf{x})$ is thereby described in terms of the local interfacial tensions $\gamma_{\mathrm{SG}}(\mathbf{x})$ and $\gamma_{\mathrm{SL}}(\mathbf{x})$ at the location $\mathbf{x}$, or, more precisely, by their fluctuation due to the presence of a chemical contamination,

$$\delta(\mathbf{x}) = \gamma_{\mathrm{SG}}(\mathbf{x}) - \gamma_{\mathrm{SL}}(\mathbf{x}) - \langle \gamma_{\mathrm{SG}} - \gamma_{\mathrm{SL}} \rangle_{\phi} \,, \tag{1}$$

where δ is the disturbance measure, γ_{ij} are the interfacial tensions, ϕ is the circumferential co-ordinate direction along the contact line, and $\langle \cdot \rangle_{\phi}$ denotes the spatial average over the circumference. The subscripts S, G and L indicate the solid, gaseous and liquid phase, respectively. The well-known Young's equation (Lenz and Lipowsky, 1998)

$$\gamma_{\mathrm{LG}} \cos \langle \theta_{\mathrm{c}} \rangle_{\phi} = \langle \gamma_{\mathrm{SG}} - \gamma_{\mathrm{SL}} \rangle_{\phi} \tag{2}$$

is locally modified due to the presence of a chemical contamination (see also Fig. 1(e)). From Eqs. (1) & (2) follows

$$\begin{aligned} \gamma_{\mathrm{LG}} \cos \theta(\mathbf{x}) &= \delta(\mathbf{x}) + \langle \gamma_{\mathrm{SG}} - \gamma_{\mathrm{SL}} \rangle_{\phi} && (3) \\ &= \gamma_{\mathrm{SG}}(\mathbf{x}) - \gamma_{\mathrm{SL}}(\mathbf{x}) \,, && (4) \end{aligned}$$

with $\theta(\mathbf{x})$ being the locally modified contact angle at the location $\mathbf{x}$ in contrast to the unperturbed contact angle θ_{c} in the absence of any contamination, see Eq. (2). Assuming the chemical contamination being small ($|\Delta\theta| = |\theta(\mathbf{x}) - \theta_{\mathrm{c}}| \ll \theta_{\mathrm{c}}$), de Gennes (1985) introduced the following expression (following from Eqs. (2) & (4)) for the change in the local equilibrium contact angle, $\Delta\theta$, at the triple phase contact line due to the presence of a chemical contamination,

$$\Delta\theta = \theta(\mathbf{x}) - \theta_{\mathrm{c}} = -\frac{\delta}{\gamma_{\mathrm{LG}} \sin \theta_{\mathrm{c}}} \,. \tag{5}$$

In the present investigation, we set $\gamma_{\mathrm{SL}} = f\gamma_{\mathrm{LG}}$, $f \in \mathbb{R}^{+}$ (without loss of generality). In the (limiting) case of the triple phase contact line being situated exactly at the border of the change in the surface properties (as depicted in Fig. 1), the local solid-liquid interfacial tension is $\gamma_{\mathrm{SL}}(\mathbf{x}) = \gamma_{\mathrm{SL}} = f\gamma_{\mathrm{LG}}$, while the local solid-gaseous interfacial tension is $\gamma_{\mathrm{SG}}(\mathbf{x}) = C(\mathbf{x})\gamma_{\mathrm{SL}} + \gamma_{\mathrm{LG}} \cos \theta_{\mathrm{c}}$, which follows from the model introduced in Eq. (11). We obtain from Eqs. (1), (10) and (11) the following expression for the chemical contamination,

$$\begin{aligned} \delta &= \gamma_{\mathrm{SG}}(\mathbf{x}) - \gamma_{\mathrm{SL}}(\mathbf{x}) - \langle \gamma_{\mathrm{SG}} - \gamma_{\mathrm{SL}} \rangle_{\phi} && (6) \\ &= \underbrace{C(\mathbf{x}) f\gamma_{\mathrm{LG}} + \gamma_{\mathrm{LG}} \cos \theta_{\mathrm{c}}}_{=\gamma_{\mathrm{SG}}(\mathbf{x})} - \underbrace{f\gamma_{\mathrm{LG}}}_{=\gamma_{\mathrm{SL}}(\mathbf{x})} - (\underbrace{f\gamma_{\mathrm{LG}} + \gamma_{\mathrm{LG}} \cos \theta_{\mathrm{c}}}_{=\gamma_{\mathrm{SG}}} - \underbrace{f\gamma_{\mathrm{LG}}}_{=\gamma_{\mathrm{SL}}}) && (7) \\ &= \gamma_{\mathrm{LG}} f\big(C(\mathbf{x}) - 1\big) \,, && (8) \end{aligned}$$

where we introduced $C(\mathbf{x}) \in \mathbb{R}$ as a model parameter for the strength of the disturbance δ (see also Eq. (11)). From Eqs. (5) & (8) follows for the deviation of the perturbed contact angle, $\theta(\mathbf{x})$, from the equilibrium contact angle in the absence of any disturbance, θ_c,

$$\Delta\theta = \frac{f(1 - C(\mathbf{x}))}{\sin\theta_c} \,. \tag{9}$$

4.2 The perturbed force equilibrium analogy

In the numerical framework described in Sec. 5.2 the local contact angle, $\theta_c(\phi)$, is imposed at the triple phase contact line as follows. A line force, $\boldsymbol{q}_c(\phi)$, is introduced, which is the contact line force balancing the liquid membrane tensions γ_{SL} and γ_{LG} acting at the contact line. This force may be split into two contributions

$$\begin{aligned} q_{c_h} &= \underbrace{\gamma_{SL} + \gamma_{LG}\cos\theta_c(\phi)}_{=\gamma_{SG}} \,, \\ q_{c_v} &= \gamma_{LG}\sin\theta_c(\phi) \,, \end{aligned} \tag{10}$$

with the subscripts h and v indicating the horizontal and vertical component of $\boldsymbol{q}_c(\phi)$, respectively (cf. Sauer (2014)). Fig. 2 (b) shows a schematic sketch of the force equilibrium at the contact line. In the case of a chemical substrate contamination with strength C at the position

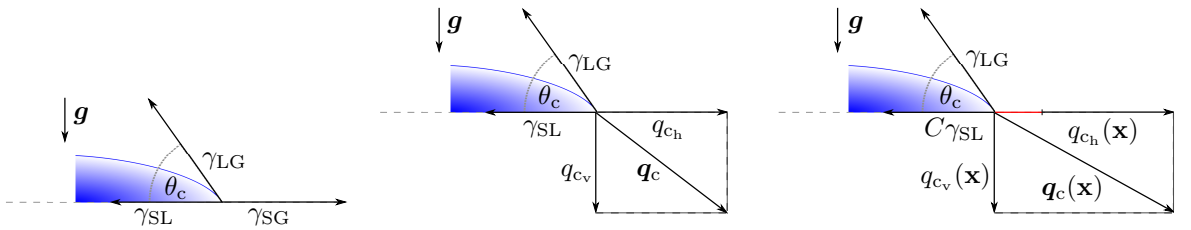

(a) Interfacial tension equilibrium (b) Force equilibrium analogy (c) Perturbed force equilibrium analogy

Figure 2: Schematic sketch of (a) the interfacial tensions γ_{ij} acting at the triple phase contact line in the absence of any chemical contamination/heterogeneity, (b) the force equilibrium analogy as considered by Sauer (2014) and (c) the perturbed force equilibrium analogy in the presence of a chemical contamination, C. The change in the horizontal part of $\boldsymbol{q}_c$ due to the chemical contamination/heterogeneity is indicated in red.

$\mathbf{x}$ the force equilibrium in horizontal direction is modified due to the presence of the contamination (see Fig. 2 (c)) and a change in the solid-gaseous interfacial tension, γ_{SG}, which is modeled by the parameter $C(\mathbf{x})$ as

$$q_{c_h}(\mathbf{x}) = \underbrace{C(\mathbf{x})\,\gamma_{SL} + \gamma_{LG}\cos\theta_c(\phi)}_{=\gamma_{SG}(\mathbf{x})} \,. \tag{11}$$

From the model for the solid-gaseous interfacial tension γ_{SG} introduced in Eq. (10) and its extension (11) an expression for the deviation in the local contact angle $\Delta\theta_F$ is derived (where the super-/subscript F stands for force),

$$\underbrace{C(\mathbf{x})\,\gamma_{SL} + \gamma_{LG}\cos\theta_c(\phi)}_{=\gamma_{SG}(\mathbf{x})} = \underbrace{\gamma_{SL} + \gamma_{LG}\cos\theta_F(\mathbf{x})}_{=\gamma^F_{SG}(\mathbf{x})} \tag{12}$$

$$C(\mathbf{x})\,f\gamma_{LG} + \gamma_{LG}\cos\theta_c(\phi) = f\gamma_{LG} + \gamma_{LG}\cos\theta_F(\mathbf{x}) \tag{13}$$

$$\gamma_{LG}\big(\cos\theta_c(\phi) - \cos\theta_F(\mathbf{x})\big) = \gamma_{LG}\big(f(1 - C(\mathbf{x})\big) \tag{14}$$

$$\implies \Delta\theta_F = \theta_F(\mathbf{x}) - \theta_c(\phi) = \arccos\big(f(C(\mathbf{x}) - 1) + \cos\theta_c(\phi)\big) - \theta_c(\phi) \,, \tag{15}$$

which is independent of the interfacial tensions γ_{ij} (due to $\gamma_{\mathrm{SL}} = f\gamma_{\mathrm{LG}}$). This is achieved by introducing the local contact angle $\theta_{\mathrm{F}}(\mathbf{x})$ resulting from the chemical heterogeneity $C(\mathbf{x})$ and equating $\gamma_{\mathrm{SG}}(\mathbf{x})$ with its counterpart $\gamma^{\mathrm{F}}_{\mathrm{SG}}(\mathbf{x})$ based on $\theta_{\mathrm{F}}(\mathbf{x})$. $\gamma_{\mathrm{SG}}(\mathbf{x})$ takes thereby the local contact angle $\theta_{\mathrm{c}}(\phi)$ in the absence of any chemical heterogeneity into account. We want to emphasize that the restriction to small chemical contaminations does not apply here, i.e. that the analytical prediction for the contact angle deviation $\Delta\theta_{\mathrm{F}}$ is valid for a much larger range of chemical contaminations compared to de Gennes (1985).

The parameter $C(\mathbf{x})$ has to be chosen as follows to guarantee physically reasonable results. For $C < 1$ the strength of the chemical contamination has to satisfy

$$\theta(\mathbf{x}) = \theta_c + \Delta\theta \leq \pi \quad \Longleftrightarrow \quad C \geq \frac{f + (\theta_{\mathrm{c}} - \pi)\sin\theta_{\mathrm{c}}}{f}\,, \tag{16}$$

$$\theta_{\mathrm{F}}(\mathbf{x}) = \theta_{\mathrm{c}} + \Delta\theta_{\mathrm{F}} \leq 180^\circ \quad \Longleftrightarrow \quad C \leq \frac{f - 1 - \cos\theta_{\mathrm{c}}}{f}\,, \tag{17}$$

and

$$\theta(\mathbf{x}) = \theta_{\mathrm{c}} - \Delta\theta \geq 0 \quad \Longleftrightarrow \quad C \geq \frac{f - \theta_{\mathrm{c}}\sin\theta_{\mathrm{c}}}{f}\,, \tag{18}$$

$$\theta_{\mathrm{F}}(\mathbf{x}) = \theta_{\mathrm{c}} - \Delta\theta_{\mathrm{F}} \geq 0^\circ \quad \Longleftrightarrow \quad C \leq \frac{f - 1 - \cos\theta_{\mathrm{c}} + 2\cos^2\theta_{\mathrm{c}}}{f}\,, \tag{19}$$

for $C > 1$, respectively. A chemical contamination $C < 1$ thereby introduces a hydrophobic heterogeneity while $C > 1$ leads to a hydrophilic heterogeneity. For $C = 1$, no chemical contamination is present and δ, $\Delta\theta$ and $\Delta\theta_{\mathrm{F}}$ are identically zero.

4.3 Cassie's law, revisited

In this section we discuss Cassie's law in the present context and show that the predicted change in the apparent contact angle is identical to the prediction derived via the perturbed force equilibrium analogy, see Sec. 4.2.

Cassie (1948) proposed a modification of the Young's equation (Lenz and Lipowsky, 1998), see Eq. (2) above, in the presence of two chemical species A and B on a chemically heterogeneous substrate,

$$\gamma_{\mathrm{LG}}\cos\theta_{\mathrm{app}} = c\left(\gamma_{\mathrm{SG}} - \gamma_{\mathrm{SL}}\right)_{\mathrm{A}} + (1-c)\left(\gamma_{\mathrm{SG}} - \gamma_{\mathrm{SL}}\right)_{\mathrm{B}}\,, \tag{20}$$

where c represents the concentration of the species A and $(1-c)$ the concentration of the species B. θ_{app} is the apparent contact angle, which is equivalent to the locally modified contact angle of the previous section, i.e. $\theta_{\mathrm{app}} \equiv \theta_{\mathrm{F}}(\mathbf{x})$. This holds true for the pattern-like heterogeneities studied here, where species A and B are not homogeneously distributed with concentrations c and $(1-c)$, but areas covered only with species A or B are separated by sharp borders. For the specific type of chemical contamination introduced in Sec. 4.2, Eq. (20) can be written as

$$\gamma_{\mathrm{LG}}\cos\theta_{\mathrm{F}} = c\,\gamma_{\mathrm{LG}}\left(f + \cos\theta_{\mathrm{A}} - f\right) + (1-c)\,\gamma_{\mathrm{LG}}\left(f(C(\mathbf{x}) - 1) + \cos\theta_{\mathrm{B}}\right) \tag{21}$$

$$= c\,\gamma_{\mathrm{LG}}\,\cos\theta_{\mathrm{A}} + (1-c)\,\gamma_{\mathrm{LG}}\left(f(C(\mathbf{x}) - 1) + \cos\theta_{\mathrm{B}}\right)\,, \tag{22}$$

for $(\gamma_{\mathrm{SL}} = f\gamma_{\mathrm{LG}})$. For $c = 1$ the substrate is perfectly homogeneous (species A only) and the apparent contact angle is identical to the prescribed contact angle $\theta_{\mathrm{F}}(\mathbf{x}) = \theta_{\mathrm{A}} = \theta_{\mathrm{c}}$. For $c = 0$

the substrate is completely homogeneously composed of species B and Eq. (22) gives

$$\gamma_{\mathrm{LG}} \cos\theta_{\mathrm{F}}(\mathbf{x}) = \gamma_{LG} \left(f(C(\mathbf{x}) - 1) + \cos\theta_{\mathrm{B}} \right) \tag{23}$$

$$\cos\theta_{\mathrm{F}}(\mathbf{x}) - \cos\theta_{\mathrm{B}} = f(C(\mathbf{x}) - 1) \tag{24}$$

$$\theta_{\mathrm{F}}(\mathbf{x}) = \arccos\left(f(C(\mathbf{x}) - 1) + \cos\theta_{\mathrm{B}} \right) \tag{25}$$

$$\Longrightarrow \Delta\theta_C = \theta_{\mathrm{F}}(\mathbf{x}) - \theta_{\mathrm{c}} = \arccos\left(f(C(\mathbf{x}) - 1) + \cos\theta_{\mathrm{c}} \right) - \theta_{\mathrm{c}} \equiv \Delta\theta_{\mathrm{F}} \,, \tag{26}$$

which is identical to the deviation in the apparent contact angle, $\Delta\theta_{\mathrm{F}}$, derived via the perturbed force equilibrium analogy, see Eq. (15) (for $\theta_{\mathrm{B}} = \theta_{\mathrm{c}}$). The fact that Eq. (22) is only symmetric for the species A and B in case $C(\mathbf{x}) = 1$ follows from the modelling approach discussed in Sec. 4.2.

We want to emphasize that Cassie's theory is intended to describe the effects of a chemically heterogeneous substrate on the apparent contact angle where the species A and B are randomly distributed. The approach followed here (see Secs. 4.1 & 4.2) is the investigation of locally perturbed substrates, either perturbed by a locally introduced chemical contamination in analogy to de Gennes (1985) or by a change in the substrate's wetting properties at a distinct location on the substrate, e.g. a structured pattern (see Fig. 1). The location of the perturbation thereby coincides with the position of the triple phase contact line. Therefore, the theory introduced by Cassie (1948) corresponds in our setup here to an axially patterned substrate where the change from species A to species B is located at the triple phase contact line. The axial patterns are thereby homogeneously composed of either species A or B, a wetting scenario also discussed theoretically in Lipowsky et al. (1999).

4.4 Comparison of $\Delta\theta$ and $\Delta\theta_{\mathrm{F}}$

In Fig. 3 the analytical predictions for $\Delta\theta$ and $\Delta\theta_{\mathrm{F}}$ are compared for chemical contaminations with a strength $0 \leq C \leq 2$. The predicted deviations $\Delta\theta$ and $\Delta\theta_{\mathrm{F}}$ from the equilibrium

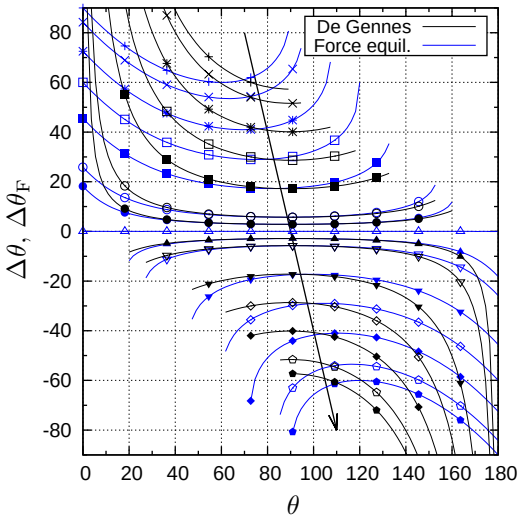

Figure 3: Comparison of the predicted deviations $\Delta\theta$ and $\Delta\theta_{\mathrm{F}}$ following from Eqs. (9) (black) & (15) (blue) for $f = 1$. Calculated values for $\Delta\theta$ and $\Delta\theta_{\mathrm{F}}$, which are larger than the maximum possible physical contact angle correction (see Eqs. (17) - (19)) are blanked out. The strength of the chemical contamination varies in $C = [0, 0.1, 0.3, \ldots, 0.9, 0.95, 1, 1.05, 1.1, 1.3, \ldots, 1.9, 2]$, which is indicated by the black arrow. Corresponding symbols in the curves denote equal C. For $C = 1$ no contamination is present and $\Delta\theta$ and $\Delta\theta_{\mathrm{F}} \equiv 0$.

contact angle θ_{c} in the presence of a chemical contamination δ are identical for a large range of

equilibrium contact angles θ_c. Even for contaminations $0.7 \leq C \leq 1.3$, where the theory given by de Gennes (1985) is already significantly stretched, a good match is observed for equilibrium contact angles $50° \leq \theta_c \leq 120°$. For weaker chemical contaminations ($0.9 \leq C \leq 1.1$), the range of θ_c, where a good match is found, is considerably larger. For very strong chemical contaminations, large differences are found in the predicted contact angle deviations $\Delta\theta$ and $\Delta\theta_F$ and different asymptotic values for small/large equilibrium contact angles θ_c are observed. While the prediction for $\Delta\theta$ tends to infinity for small/large equilibrium contact angles ($\theta_c \to 0° \Rightarrow \Delta\theta \to +\infty; \theta_c \to 180° \Rightarrow \Delta\theta \to -\infty$), the prediction for $\Delta\theta_F$ derived from the perturbed force equilibrium analogy (Eq. (15)) is bounded for all $\theta_c \in [0°, 180°]$. This property of the prediction for $\Delta\theta_F$ is a result of the generality of its derivation, which does not include any restrictions for the strength of the chemical contamination, δ, nor the contact angle deviation, $\Delta\theta_F$, relative to the equilibrium contact angle, θ_c.

As we will discuss in detail in Sec. 6, the predictions for $\Delta\theta$ and $\Delta\theta_F$ made in Eqs. (9) & (15) can be used to transform the results obtained by means of numerical simulations for the shape of droplets on contaminated substrates to (analytical) reference solutions in the absence of any perturbation. This opens up the possibility to evaluate the accuracy of experimental as well as numerical results for the wetting on chemically contaminated substrates against well-known results obtained for perfectly homogeneous substrates.

5 Numerical framework

In this section, we introduce the equations governing the physics of sessile droplets on rigid substrates (Sec. 5.1). Furthermore, we present briefly the numerical framework utilized in the present investigation (Sec. 5.2) as well as the simulation setup (Sec. 5.3). The description and nomenclature herein follows closely Sauer et al. (2014). Therefore, we refer to Sauer et al. (2014) for details on the membrane kinematics in curvilinear coordinates as well as on the constraint formulation. For an introduction to the nonlinear finite elements and computational contact algorithms we refer to the textbooks by Wriggers (2008, 2006).

5.1 Governing equations

The present investigation deals with the partial wetting on substrates by sessile droplets, represented by a liquid membrane, on a rigid substrate. The governing equations are non-dimensionalized using the initial droplet radius, R_0°, the density of water, ρ_w°, the liquid-gaseous interfacial tension, γ_{LG}°, and the gravitational acceleration, $\boldsymbol{g} \hat{=} (0, 0, g^\circ)^T$, where $(\cdot)^\circ$ denotes dimensional quantities. The Bond number is defined as $Bo = g^\circ \rho_w^\circ R_0^{\circ 2} / \gamma_{LG}^\circ$ and sets gravitational and surface tension effects into relation.

The nonlinear deformation of an incompressible, liquid membrane is described by the following equation following from the balance of linear momentum (strong equilibrium form)

$$\boldsymbol{t}^\alpha_{;\alpha} + \boldsymbol{f} = \boldsymbol{0}\,, \tag{27}$$

where $\boldsymbol{t}^\alpha = \boldsymbol{\sigma}\,\boldsymbol{a}^\alpha$ denotes the internal traction with $\boldsymbol{a}^\alpha, \alpha = 1, 2$ being the contra-variant base vectors of the tangent plane at a specific location on the membrane, and $\boldsymbol{\sigma} = \sigma^{\alpha\beta}\boldsymbol{a}_\alpha \otimes \boldsymbol{a}_\beta$ is the Cauchy stress tensor considered to be symmetric and $\mathbf{a}_\alpha$ the co-variant basis of the tangent plane. Here $\boldsymbol{f} = f_\alpha\,\boldsymbol{a}^\alpha + p\,\boldsymbol{n}$ is a distributed surface force where f_α is the co-variant in-plane component of $\boldsymbol{f}$ and p is the out-of-plane pressure acting on the membrane.

The droplet is assumed to be in a state of hydrostatic equilibrium and is therefore represented by a liquid membrane under internal hydrostatic pressure at constant volume (volume constraint). The volume is constrained due to assuming the liquid to be incompressible. The pressure is decomposed in its hydrostatic part, p_h, and its part due to the volume constraint, p_v,

$$p = p_\mathrm{h} + p_\mathrm{v} = \rho_\mathrm{w}\, \boldsymbol{g} \cdot \boldsymbol{x} + p_\mathrm{v}\,, \tag{28}$$

where ρ_w is the density of water and $\boldsymbol{x}$ the position vector in 3D space. The value of the volumetric pressure, p_v, is the constant datum pressure at the origin.

The liquid membrane is subject to the usual Dirichlet and Neumann boundary conditions,

$$\boldsymbol{u} = \overline{\boldsymbol{u}} \qquad \text{on } \partial_u S\,, \qquad \boldsymbol{t} = \bar{\boldsymbol{t}} \qquad \text{on } \partial_t S \tag{29}$$

on the membrane boundary $\partial S = \partial_u S \cup \partial_t S$ to close the problem, where $\boldsymbol{u}$ denotes the membrane displacement.

The material properties of the liquid membrane are governed by the constant isotropic surface tension γ_{ij}, such that the membrane stress becomes

$$\sigma^\alpha_\beta = \gamma_{ij}\, \delta^\alpha_\beta\,, \tag{30}$$

with δ^α_β being the Kronecker symbol.

5.2 Numerical methods

In this section the numerical method is presented, which is used throughout the present investigation.

The droplet (and its deformation) is represented by a flexible, liquid membrane in the present investigation. To this end, the weak form of Eq. (27) (see Sauer et al. (2014) for details) is discretized using quadratic Lagrange finite elements. The liquid membrane is stabilized in-plane following Sauer (2014) (stabilization scheme 'P'). The simulations are load-driven by sequentially increasing the gravitational load, $\boldsymbol{g}$, and the contact line force, $\boldsymbol{q}_\mathrm{c}$, to its maximum value and solving for the quasi-static equilibrium deformation at every load increment. The liquid droplet is thereby subject to a volume and contact constraints. Its fluid phase in the interior is represented by the hydrostatic pressure distribution (Eq. (28)) acting on the membrane surface. The resulting linear system of equations is solved using the Newton-Raphson iteration (which implies solving a linear system at each iteration step) subject to boundary and symmetry conditions, see Sec. 5.3.

The contact between the liquid droplet and the rigid infinite half-space is modeled frictionless. The contact pressure is thereby determined by a penalty regularization based on the classical contact constraint, see Sauer (2014) for details.

5.3 Simulation setup

Fig. 4 shows the simulation setup used throughout the present investigation at initialization. The droplet, represented as a liquid membrane, is in contact with a rigid, infinite half-space with its surface located at $z = -R_0$. The initial droplet radius is R_0, the droplet is represented by one quarter of a sphere exploiting thereby the following symmetry conditions to increase the computational efficiency of the simulations,

$$u_x = 0 \quad \text{at } x = 0\,, \qquad u_y = 0 \quad \text{at } y = 0\,. \tag{31}$$

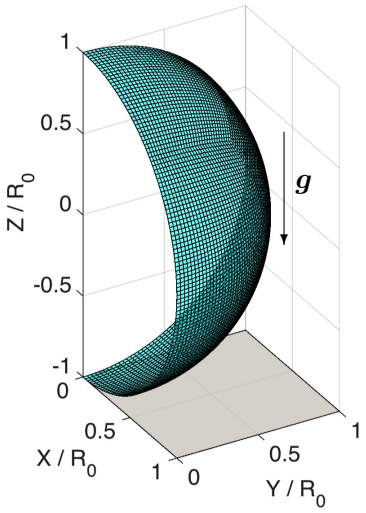

Figure 4: Simulation setup. Initial configuration of the droplet. Rigid substrate (half-space) indicated in grey, either homogeneous or heterogeneously patterned as indicated in Fig. 1. Gravity acting in the negative z-direction indicated by the vertical arrow.

The initial volume of the droplet, $V_0 = 1/3\pi R_0^3$, is kept constant throughout the simulations (volume constraint). The gravitational pull acts in negative z-direction, $\boldsymbol{g} \hat{=} (0, 0, -g)^{\mathrm{T}}$. The contact angle, θ_{c}, is varied in the range $[45°, 150°]$, the Bond number, Bo, in the range $[0, 5]$ and the strength of the chemical contamination, C, in the range $[0, 2]$.

The simulations run with the total number of $n_{\mathrm{el}} = 12,352$ quadratic elements, leading to a total number of $n_{\mathrm{no}} = 24,833$ nodes. The total number of elements contains membrane elements, representing the liquid droplet, contact surface elements, and contact line elements. The contact line elements, situated at the equator of the droplet, allow for imposing the contact force $\boldsymbol{q}_{\mathrm{c}}$ introduced in Eqs. (10) & (11). The total number of degrees of freedom is $n_{\mathrm{dof}} = 74,500$. The grid resolution is sufficiently high to guarantee accurate, grid-independent numerical results. The load-stepping is chosen dynamically to accelerate the simulations and to reduce the turn-around time per parameter set (θ_c, Bo, C).

6 Numerical results

In this section we present the numerical results obtained by applying the numerical framework introduced in Sec. 5 to the case of wetting on chemically contaminated substrates. We will present results for the case of zero gravity and chemically heterogeneous substrates ($Bo = 0, C \neq 1$) in Sec. 6.1 and will extend the analysis to Bond numbers $Bo > 0$ in Sec. 6.2. Wetting scenarios are considered where the entire triple phase contact line is affected by the chemical heterogeneity (see Fig. 1). Comparisons to analytical results are made where possible and the validity of the mapping based on the predicted contact angle deviation is shown. Furthermore, we will show the applicability of the numerical approach to generalized chemical contaminations, where only some part of the triple phase contact line is affected (Sec. 6.3).

6.1 Axially patterned substrates in the absence of gravity ($Bo = 0$)

The advantage of investigating the wetting of droplets on rigid substrates in the absence of gravity, i.e. for the Bond number $Bo = 0$, is the availability of analytical results for the wetting radius, r, the wetting length, L, and the droplet height, h, at the hydrostatic equilibrium

state, which are used as an exact benchmark in the present investigation. In the absence of gravity (and C constant in r and ϕ), the droplets form spherical caps (de Gennes, 1985). The well-known solution for the droplet radius, $r(\theta_c)$, for $Bo = 0$ at the equilibrium state is

$$r(\theta_c) = R_0 \cdot \left(\frac{4}{2 + \cos^3 \theta_c - 3 \cos \theta_c} \right)^{\frac{1}{3}} , \tag{32}$$

with R_0 the initial droplet radius and θ_c the equilibrium contact angle. The droplet height, $h(\theta_c)$, is then defined as

$$h(\theta_c) = r(\theta_c) \cdot (1 - \cos \theta_c) \tag{33}$$

and the wetting length, $L(\theta_c)$, is

$$L(\theta_c) = 2 \cdot r(\theta_c) \cdot \sin \theta_c \, . \tag{34}$$

In the presence of a chemical contamination of strength $C = C(r)$ affecting the entire triple phase contact line (axial pattern), the contact angle $\theta_c(r)$ at the triple phase contact line changes according to Eqs. (9) & (15), respectively. Following from the change in the contact angle, $\theta_c + \Delta\theta$ and $\theta_c + \Delta\theta_F$, respectively, the shape of the droplet changes as well, assuming a constant droplet volume and further that no contact line pinning takes place. The radius, r, the wetting length, L, and the height, h, of the droplet may be calculated analytically by replacing θ_c in Eqs. (32) - (34) with the modified value $\theta_c + \Delta\theta$ and $\theta_c + \Delta\theta_F$, respectively, due to the presence of the chemical contamination. This results in analytical expressions for the shape of the droplet, which depend on the strength of the chemical contamination, C.

Fig. 5 shows the numerical results for the droplet height, h, and the wetting length, L, at hydrostatic equilibrium and compares the results with the analytical solutions for the modified contact angle, $\theta_c + \Delta\theta$, according to Eq. (9) and $\theta_c + \Delta\theta_F$ according to Eq. (15). For the absence of any chemical contamination ($C = 1$) the numerical results perfectly match the analytical solutions according to Eqs. (33) & (34) re-verifying thereby the accuracy of the numerical method, cf. (Sauer, 2014). The droplet height, h, increases for chemical contaminations $C < 1$ and decreases for $C > 1$ in accordance with the deviations of the contact angle, see Fig. 3, which are predicted to be $\Delta\theta > 0$ for $C < 1$ and $\Delta\theta < 0$ for $C > 1$, respectively. For the wetting length, L, the opposite trend is observed: chemical contaminations $C < 1$ lead to a decrease in the wetting length while for $C > 1$ the spreading of the droplet is enhanced. Since the chemical contamination affects the entire triple phase contact line, the wetting area, or the contact area between the droplet and the rigid substrate, remains circular. The droplet shape is a spherical cap due to the absence of gravity $Bo = 0$.

The analytical solutions modified according to the theory by de Gennes (1985), see Eq. (9) above, show good agreement with the numerical results for small chemical contaminations $0.7 < C < 1.3$. For stronger chemical contaminations larger deviations between the numerical results and the modified analytical solutions are observed reflecting the limitations of the theory by de Gennes (1985). For very small and large equilibrium contact angles, θ_c, the analytical solutions start to oscillate due to the unboundedness of the deviation, $\Delta\theta$, and a comparison to the numerical results is not reasonable anymore.

Since the predicted deviation $\Delta\theta_F$ derived from the perturbed force equilibrium analogy, Eq. (15), is bounded for all $0° \leq \theta_c \leq 180°$ the modified analytical solutions for the droplet height, h, and the wetting length, L, show a monotonic behavior over the entire parameter range. The agreement between the modified analytical solutions and the numerical results is nearly perfect, independent of the strength of the chemical contamination, C, and the contact angle, θ_c. The excellent agreement demonstrates the generality of the perturbed force equilibrium analogy, Eq. (15), and verifies the numerical framework utilized.

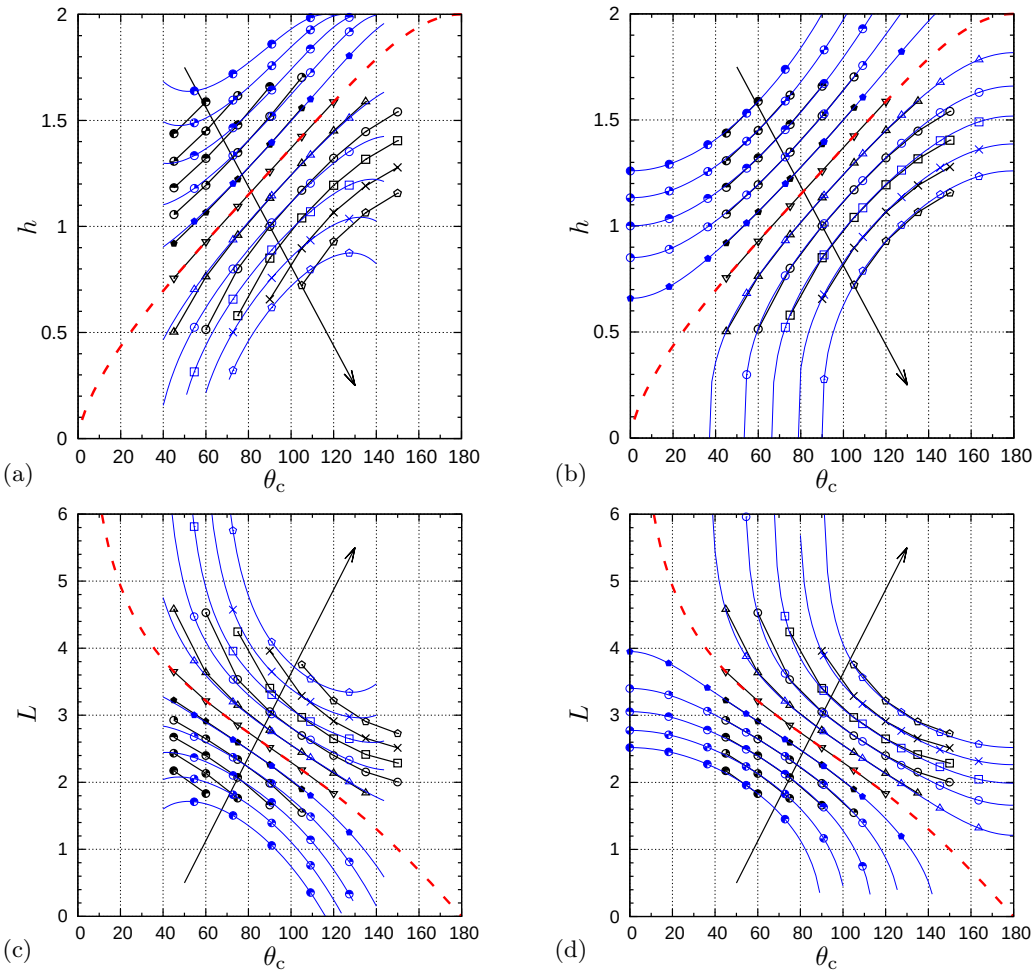

Figure 5: Numerical results for the droplet height, h, and the wetting length, L, for $Bo = 0$ (black). The analytical predictions according to Eqs. (33) & (34) are calculated using (a,c) $\theta_c + \Delta\theta$ according to Eq. (9) and (b,d) $\theta_c + \Delta\theta_F$ according to Eq. (15) (blue). The analytical result in the absence of any contamination, ($C = 1$), is plotted in red. The strength of the contamination varies in $C = [0, 0.2, \ldots, 2]$, which is indicated by the black arrow. Lines with identical symbols correspond to each other.

6.2 Axially patterned substrates in the presence of gravity ($Bo \neq 0$)

In this section, we extend the numerical analysis presented in Sec. 6.1 to the general case of the presence of gravity ($0 < Bo \leq 5$). The applicability of the contact angle deviation $\Delta\theta_F$ predicted by the force equilibrium analogy (Eq. (15)) to results in the presence of gravity is demonstrated.

Fig. 6 depicts the numerical results for the droplet height and the wetting length for $Bo = \{1, 2, 5\}$. For identical contact angles, θ_c, the droplet height is lower and the wetting length is larger in the presence of gravity compared to the case $Bo = 0$. As expected from the results discussed in the previous section (Sec. 6.1), the droplet height decreases for chemical contaminations $C < 1$ and increases for $C > 1$, while for the wetting length the trend is opposite. In the presence of a chemical contamination ($C \neq 1$), the numerical results for an imposed contact angle θ_c can be shifted by the predicted contact angle deviation $\Delta\theta_F$ (Eq. (15)), such that they match the results for the case of an absence of any chemical contamination:

$$\forall\, \theta_c \in [0°, 180°], C, Bo \in \mathbb{R}_0^+ : \begin{cases} h(\theta_c + \Delta\theta_F, C, Bo) = h(\theta_c, C = 1, Bo)\,, \\ L(\theta_c + \Delta\theta_F, C, Bo) = L(\theta_c, C = 1, Bo)\,. \end{cases} \tag{35}$$

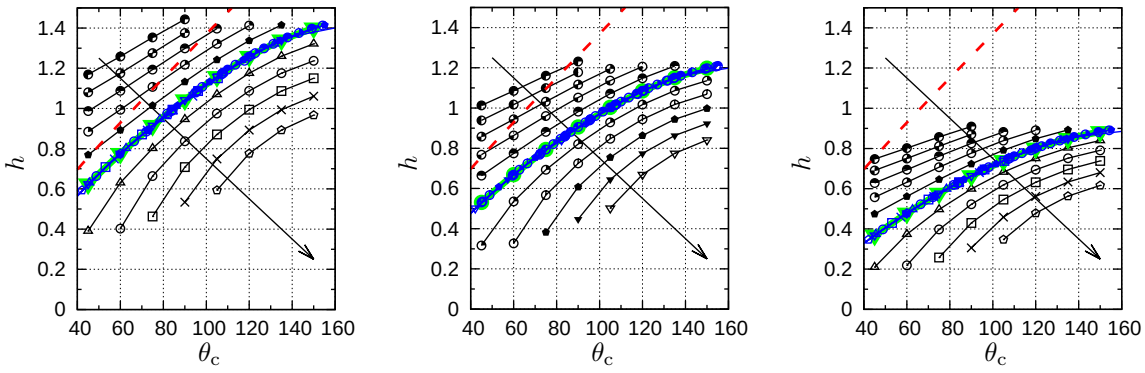

(a) Droplet height

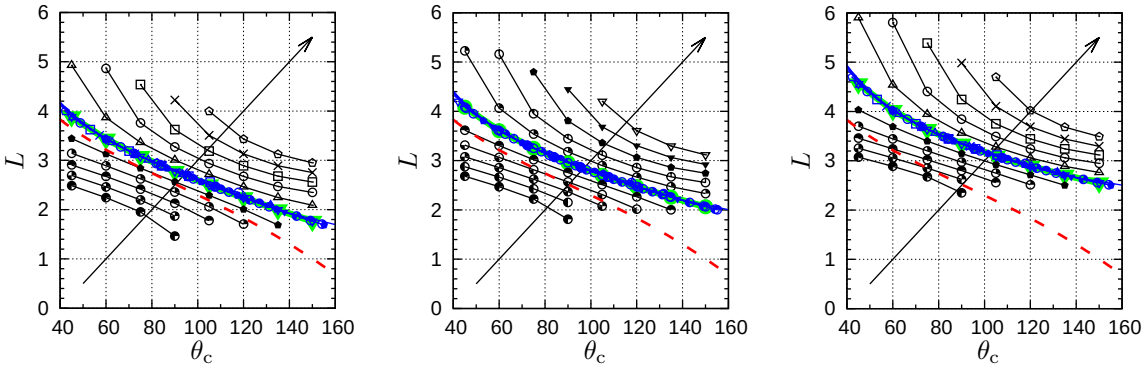

(b) Wetting length

Figure 6: Numerical results for the droplet height, h, and the wetting length, L, for $Bo = \{1, 2, 5\}$ (black, left-to-right) for $C = [0, 0.2, \ldots, 2]$. The strength of the contamination increases in the direction of the black arrow. The analytical solution for $Bo = 0$, $C = 1$ is plotted in red, the numerical results for $Bo = \{1, 2, 5\}$, $C = 1$ are plotted in green. The blue lines show the numerical results shifted by $\Delta\theta_F$ according to Eqs. (15) & (35). Lines with identical symbols correspond to each other.

The numerical results in the presence of a chemical contamination ($C \neq 1$) shifted according to Eqs. (15) & (35) coincide with the results obtained in the absence of any perturbation ($C = 1$). It is concluded from this observation that in the case of a chemical contamination affecting the entire triple phase contact line (axial pattern) the shape of a droplet wetting a rigid substrate may be calculated based on theoretical predictions, provided the wetting state on a perfectly homogeneous substrate ($C = 1$) is known.

Fig. 7 shows the results for the dimensionless shape parameters X, Y introduced in Yonemoto and Kunugi (2014):

$$1 = \underbrace{\frac{2\pi r^2}{hV}\frac{\gamma_{LG}(1-\cos\theta_c)}{\rho_w g}}_{X} - \underbrace{\frac{2\pi r}{V}\frac{\gamma_{LG}\sin\theta_c}{\rho_w g}}_{Y}. \tag{36}$$

For an increasing initial equilibrium contact angle, θ_c, the shape factors X and Y decrease. For strong chemical contaminations the shape parameters are significantly smaller ($C < 1$), or larger ($C > 1$), as for the case of a chemically homogeneous substrate. The observed change in the shape parameters is larger for X than for Y because of the stronger impact of the chemical contamination on the wetting length compared to the droplet height (see Fig. 6) and its quadratic contribution in the enumerator of X, see Eq. (36). Applying the mapping introduced in Eqs. (15) & (35) to the results for X and Y for $C \neq 1$ obtained by numerical simulations, we find coincidence with the results for $C = 1$ in the case of a homogeneous substrate. This result gives further evidence of the generality of the mapping. The effect of a chemical contamination $C > 1$ decreases for an increasing Bond number because of the relatively

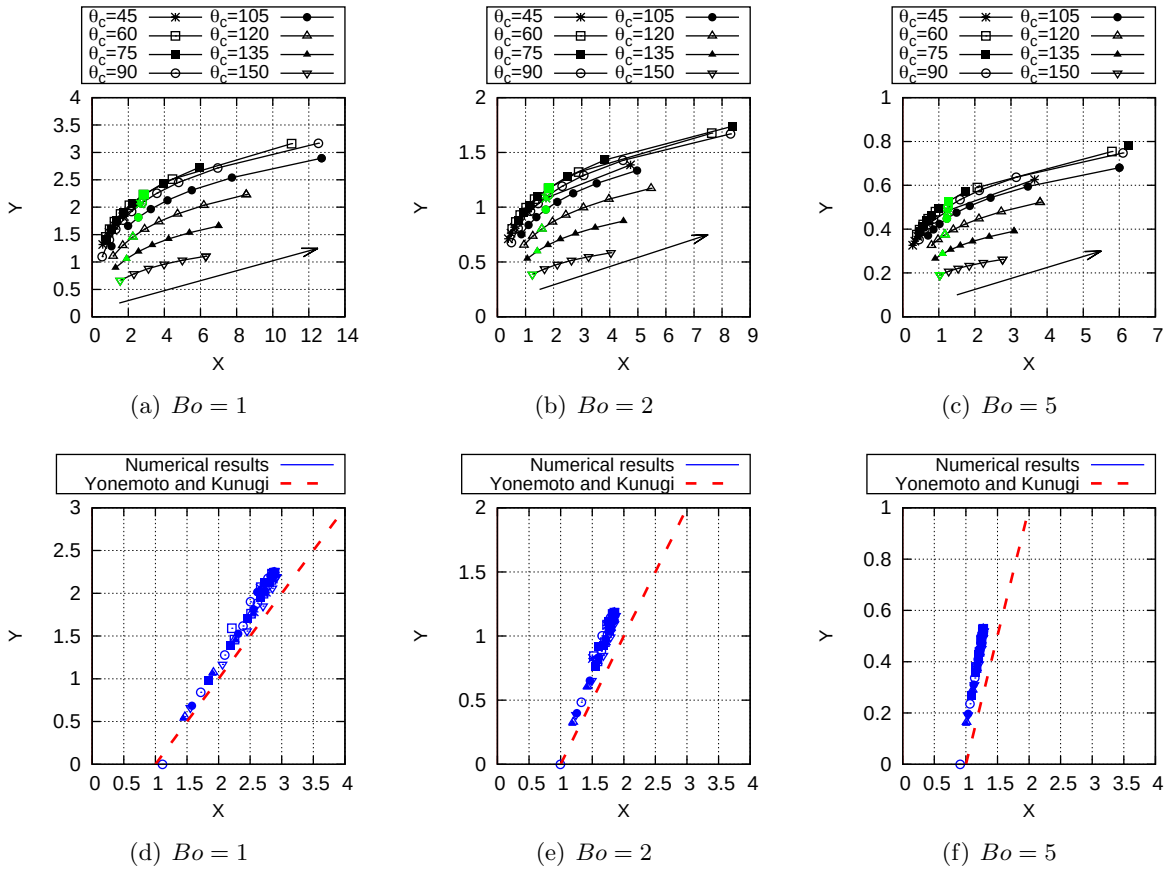

(a) $Bo = 1$ (b) $Bo = 2$ (c) $Bo = 5$

(d) $Bo = 1$ (e) $Bo = 2$ (f) $Bo = 5$

Figure 7: Numerical results for the non-dimensional shape parameters X and Y as defined in Yonemoto and Kunugi (2014) for different initial contact angles θ_c. (a-c) The numerical results for $Bo = \{1, 2, 5\}$ and varying C are plotted in black, the results for $C = 1$ are plotted in green. The strength of the contamination varies in $C = [0, 0.2, \ldots, 2]$, which is indicated by the black arrow. (d-f) The blue symbols show the numerical results shifted by $\Delta\theta_F$ according to Eqs. (15) & (35). The analytical solution $Y = X - 1$ of Yonemoto and Kunugi (2014) is plotted in red.

minor change in the wetting length (or wetting radius) compared to the homogeneous case. The relative increase in Y for a varying chemical contamination C shows a similar but weaker trend. The agreement of the results with the wetting model of Yonemoto and Kunugi (2014) in the absence of any chemical heterogeneity is good with a slight trend towards smaller deviations for larger Bond numbers. The observed deviations are in the same order of magnitude as the differences between experimental results and the model predictions reported in Yonemoto and Kunugi (2014, esp. Fig. 4). The trend towards smaller deviations for larger Bond numbers found in the present investigation may be explained by the model's approximation of the gravitational point with a height average. This approximation becomes exact for more pancake-like shaped droplets, i.e. large Bond numbers, which is reflected by the stronger agreement between the model and the present results.

In the absence of any chemical contamination ($C = 1$) the 3D shapes of the droplets are more and more pancake-shaped compared to the caps observed in the absence of gravity ($Bo = 0$) as expected (not shown for brevity). The chemical contamination has the same effect on the wetting behavior of the droplet as for the case of $Bo = 0$. The wetting area remains circular due to the contamination acting on the entire triple phase contact line (axial pattern), in contrast to the observations made in Sec. 6.3 (axial-radial pattern).

6.3 Axially-radially patterned substrates ($Bo = 1$)

In this section the chemical contaminations are applied to parts of the triple phase contact line only. The scenarios correspond thereby to the cases depicted in Fig. 1(b,d,e). The contaminations applied affect only some part of the triple phase contact line $0 \leq \phi \leq \Phi_\mathrm{p}$, where Φ_p defines the part of the contact line being affected:

$$C(\phi) := \begin{cases} \neq 1 & \text{for} \quad 0 \leq \phi \leq \Phi_\mathrm{p}\,, \\ = 1 & \text{else}\,. \end{cases} \tag{37}$$

Here, the angle Φ_p is defined for the initial droplet configuration depicted in Fig. 4. Therefore, the part of the triple phase contact line being affected by the wettability change does not change during the simulation but may stretch or compress due to contact line deformation. As a consequence, the actual patch angle, ϕ_p, may be larger for contaminations $C \gg 1$ and smaller for contaminations $C \ll 1$, respectively. As discussed below, this effect may be of importance for strong contaminations C. Nevertheless, good agreement to results reported in literature is found as shown in Fig. 9(e).

The larger Φ_p, i.e. the part of the contact line affected by the contamination, the stronger the increasing ($C < 1$) or decreasing effect ($C > 1$) on the droplet height. The limiting cases are thereby the absence of any chemical contamination ($\Phi_\mathrm{p} = 0$) and a fully affected contact line $\Phi_\mathrm{p} = 90°$ already discussed in Sec. 6.2. Fig. 8 shows top-view plots of the droplet radius at equilibrium state, i.e. the shape of the wetting area. Depending on the type of contamination, the equilibrium contact angle increases or decreases and the wetting radius is smaller or larger, respectively, compared to the case of a homogeneous substrate. Since the triple phase contact line is affected only partially by the contamination, the wetting area is not circular anymore and the wetting radius depends on the circumferential coordinate ϕ. The larger Φ_p and C the stronger the deviation from the circular wetting area observed for the homogeneous case ($C = 1$). For moderate chemical contaminations $C = 1 \pm 0.2$, the wetting area is ellipsoidally shaped, with the shorter axis aligned with the x-axis for $C < 1$ and with the y-axis for $C > 1$, respectively. For stronger chemical contaminations, the deformation of the wetting area is obviously stronger and a saddle or shoulder develops in the vicinity of $\phi = \Phi_\mathrm{p}$ comparable to observations reported in Dupuis and Yeomans (2004).

In the vicinity of $\phi = \phi_\mathrm{p}$ the apparent contact angle, θ_app, changes from the value $\theta_\mathrm{c} + \Delta\theta_\mathrm{F}$ to the initially set value θ_c, which is shown exemplarily in Fig. 8(f) for the case of $\Phi_\mathrm{p} = 45°$, $\theta_c = 105°$ and $C = 1.6$. Since the patch angle Φ_p is defined in the initial configuration at $t = 0$ the actual patch angle ϕ_p is larger than Φ_p due to contact line stretching and the contact angle transition takes place at a location slightly off the initial patch border. The change in the patch size is approximately $+1.5°$ and can be neglected compared to the initial patch size $\Phi_\mathrm{p} = 45°$. This observation can be generalized: the contact line stretching (or compression) plays a minor role for moderately strong chemical contaminations and leads to significant changes in the patch size for very high/low values of C only (with a stronger effect for high values compared to low values of C). While the relative change in the patch size is small for large initial patch angles (independent of C), it is obviously larger for small values of Φ_p and strong heterogeneities as shown in Fig. 10.

The change in the apparent contact angle takes place in an abrupt manner corresponding to the sharp transition of the wetting properties on the chemically heterogeneous substrate. This observation is in agreement with numerical findings reported in Buehrle et al. (2002), who showed that the gradient of the apparent contact angle is independent of $\Delta\theta_\mathrm{F}$ for small wettability contrasts. Furthermore, the authors found that the gradient of the apparent contact

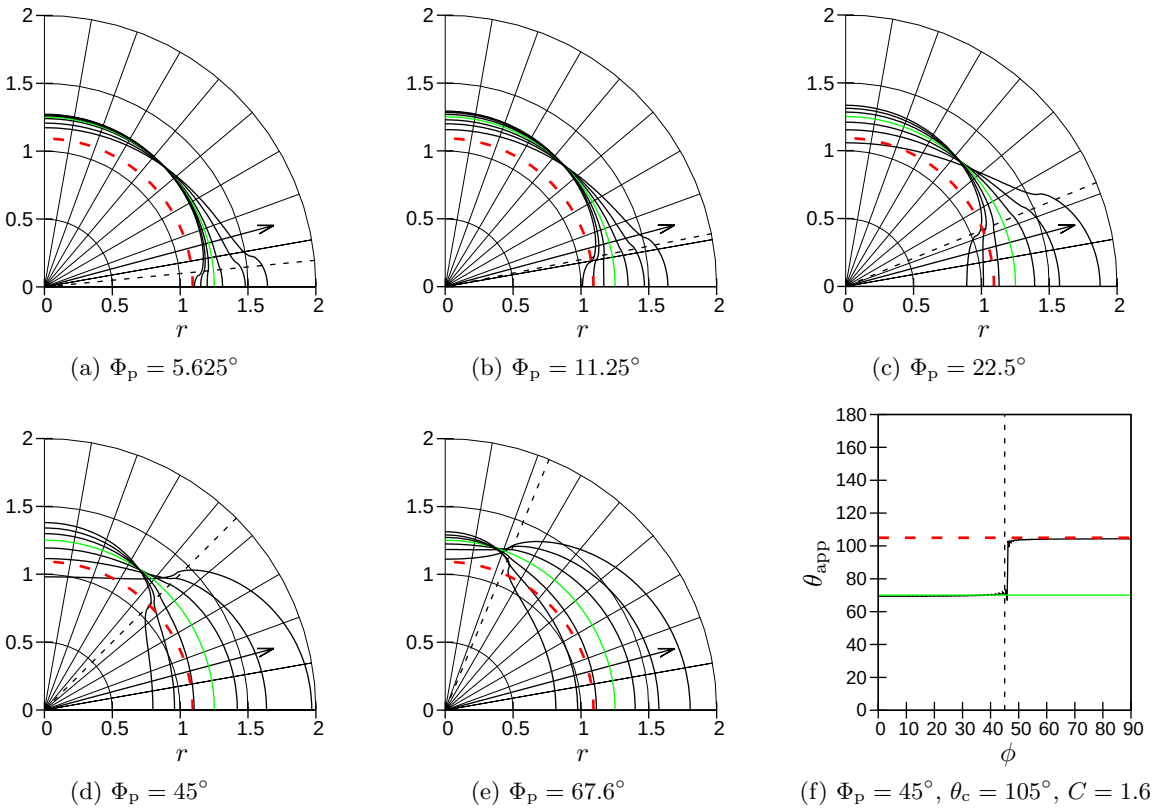

(a) $\Phi_\mathrm{p} = 5.625°$ (b) $\Phi_\mathrm{p} = 11.25°$ (c) $\Phi_\mathrm{p} = 22.5°$

(d) $\Phi_\mathrm{p} = 45°$ (e) $\Phi_\mathrm{p} = 67.6°$ (f) $\Phi_\mathrm{p} = 45°$, $\theta_\mathrm{c} = 105°$, $C = 1.6$

Figure 8: (a-e) Results for $r(\phi)$ for $Bo = 1$ (black) in the presence of an axially-radially patterned chemical contamination with $\Phi_\mathrm{p} = \{5.625, 11.15, 22.5, 45, 67.5\}[°]$ and an initial contact angle $\theta_c = 105°$. The analytical solution for $Bo = 0$, $C = 1$ is plotted in red, the numerical results for $Bo = 1$, $C = 1$ are plotted in green. The strength of the contamination varies in $C = [0.4, 0.6, \ldots, 1.6]$, which is indicated by the black arrow. The dashed black line indicates the initial patch angle Φ_p. (f) Result for the apparent contact angle $\theta_\mathrm{app}(\phi)$ for $\Phi_\mathrm{p} = 45°$, $\theta_c = 105°$ and $C = 1.6$. The dashed red line marks the initial contact angle $\theta_\mathrm{c} = 105°$, the green line $\theta_\mathrm{c} + \Delta\theta_\mathrm{F}$ according to Eq. (15).

angle is stronger for a smaller contact line tension supporting the present observations even further since the contact line tension is zero here.

As already mentioned by Iliev and Pesheva (2003), the contact angle change at the patch borders is highly sensitive to the physical mechanism of contact line pinning. In the present investigation we made similar observations, namely that the contact line in the direct vicinity of a change in the substrate's wettability properties aligns with the patch borders. The part of the triple phase contact line being aligned with the patch borders shows apparent contact angles $\theta_\mathrm{c} \leq \theta_\mathrm{app} \leq \theta_\mathrm{c} + \Delta\theta_\mathrm{F}$ as expected. The contact angle transition is accompanied by slight gridpoint-to-gridpoint oscillations, which can be minimized by increasing the spatial resolution. The result for the apparent contact angle verifies the capabilities of the utilized contact-mechanical approach to properly represent the wetting physics in the presence of heterogeneous substrates.

In the following the effects of a radially-patterned substrate on the droplet shape are investigated and compared to results presented in the previous paragraphs as well as results reported in the literature. In contrast to the results in Secs. 6.1 & 6.2 the pattern of the substrate is now defined as

$$C := \begin{cases} \neq 1 & \text{for} \quad (i-1)\Phi_\mathrm{p} - \frac{\Phi_\mathrm{p}}{2} \leq \phi \leq i\,\Phi_\mathrm{p} - \frac{\Phi_\mathrm{p}}{2}\,, \quad i = 1, 3, \ldots, \frac{90°}{\Phi_\mathrm{p}} + 1\,, \\ = 1 & \text{else} \end{cases} \tag{38}$$

resulting in a circumferentially alternating wettability pattern (dartboard pattern). The example for $\Phi_\mathrm{p} = 5.625°$ is shown in Fig. 10. This study additionally shows the capabilities of the

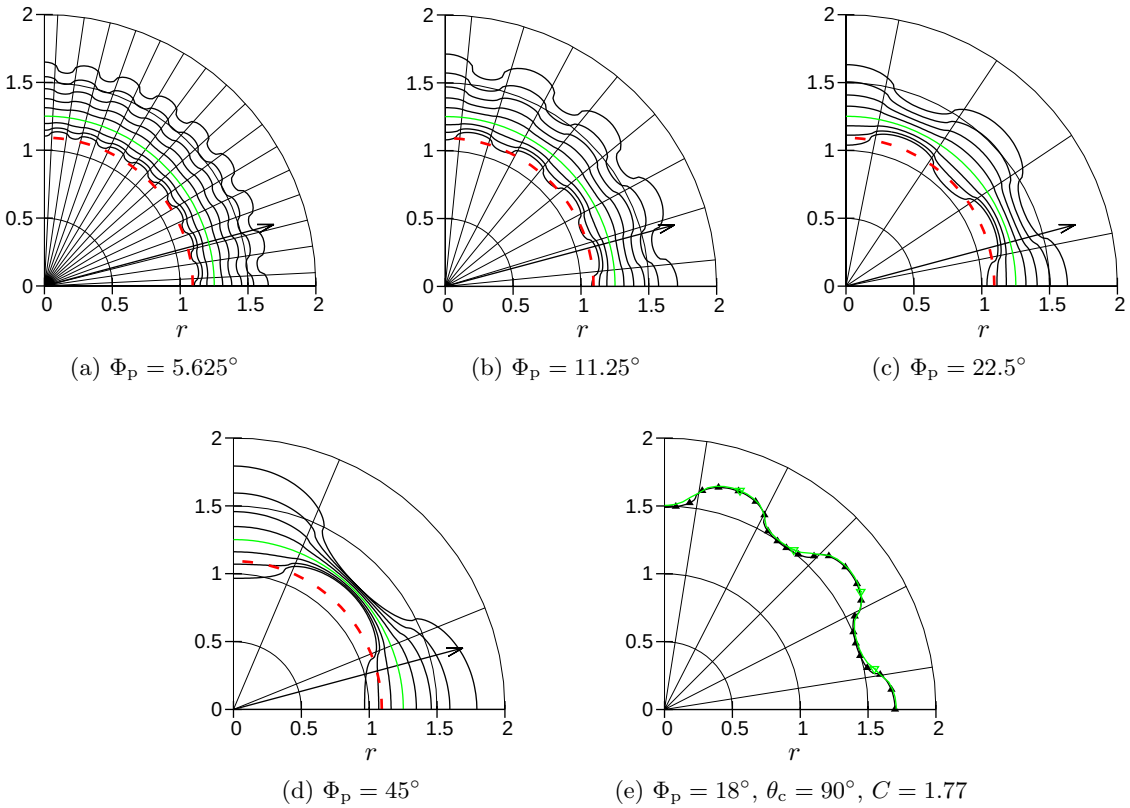

(a) $\Phi_p = 5.625°$ (b) $\Phi_p = 11.25°$ (c) $\Phi_p = 22.5°$

(d) $\Phi_p = 45°$ (e) $\Phi_p = 18°$, $\theta_c = 90°$, $C = 1.77$

Figure 9: (a-d) Results for $r(\phi)$ for $Bo = 1$ (black) in the presence of a dartboard-patterned chemical contamination with $\Phi_p = \{5.625, 11.15, 22.5, 45\}[°]$ and an initial contact angle $\theta_c = 105°$. The analytical solution for $Bo = 0$, $C = 1$ is plotted in red, the numerical results for $Bo = 1$, $C = 1$ are plotted in green. The strength of the contamination varies in $C = [0.4, 0.6, \ldots, 1.8, (2.0)]$, which is indicated by the black arrow. The grid-lines correspond to the initial patch borders. (e) Quantitative comparison between results by Iliev and Pesheva (2003) (green) and current results (black).

numerical method utilized in the present investigation.

Due to the radially-patterned nature of the chemical heterogeneity the part of the triple phase contact line being affected is approximately identical for different values of Φ_p. Therefore, the results for the droplet height do not change significantly but show a slight trend towards smaller values of h for larger angles Φ_p at constant chemical contaminations C (not shown for brevity). Compared to the results for the radially-patterned substrate according to Eq. (37) discussed in the previous paragraphs the effects of the contamination for a substrate according to Eq. (38) is stronger for identical values of Φ_p. This is due to the repeated alternation of the substrate's wetting properties in the circumferential direction leading to a larger droplet's contact area affected by the substrate heterogeneity.

The larger the contamination angle Φ_p the stronger the triple phase contact line deviation (at constant C) from the circular shape observed in the absence of any contamination, see Fig. 9(a-d). The circular shape of the wetting area is maintained for the dartboard-patterned substrate with a superimposed wave-like modulation in the circumferential direction. The wave-length of the modulation is thereby $\lambda = 2\phi_p$ in general and corresponds to the substrate's pattern. The contact line deformation as well as the 3D shape of the droplets depicted in Fig. 10 is in qualitative agreement with results reported in Dupuis and Yeomans (2004) and Iliev and Pesheva (2003). Furthermore, Fig. 9(e) shows a quantitative comparison of present results for the wetting radius with results obtained by an energy minimization procedure (Iliev and Pesheva, 2003). The agreement is generally good with slightly higher deviations on the patches

with hydrophobic wetting properties. For the present results the apparent contact angle is $\theta_{\text{app}} = 89.5°$ on the hydrophobic patches, while for the results reported in Iliev and Pesheva (2003) $\theta_{\text{app}} \approx 87°$ due to a relatively low resolution (computing power restrictions at that time). The deviation in the apparent contact angle leads to a larger wetting radius compared to the present results, which is a physically intuitive consequence. In contrast, on the substrate patches with a hydrophilic coating the apparent contact angle is $\theta_{\text{app}} = \theta_c + \Delta\theta_F \approx 40.2°$ for the present results and $\theta_{\text{app}} \approx 40.7°$ for the reference results (Iliev and Pesheva, 2003) and nearly no deviations are observed for the wetting radius.

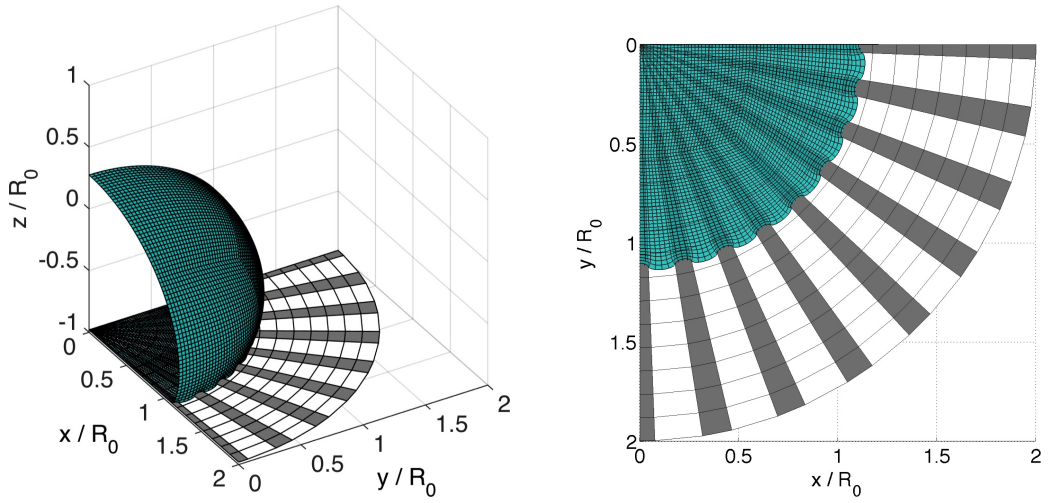

(a) $C = 0.4$

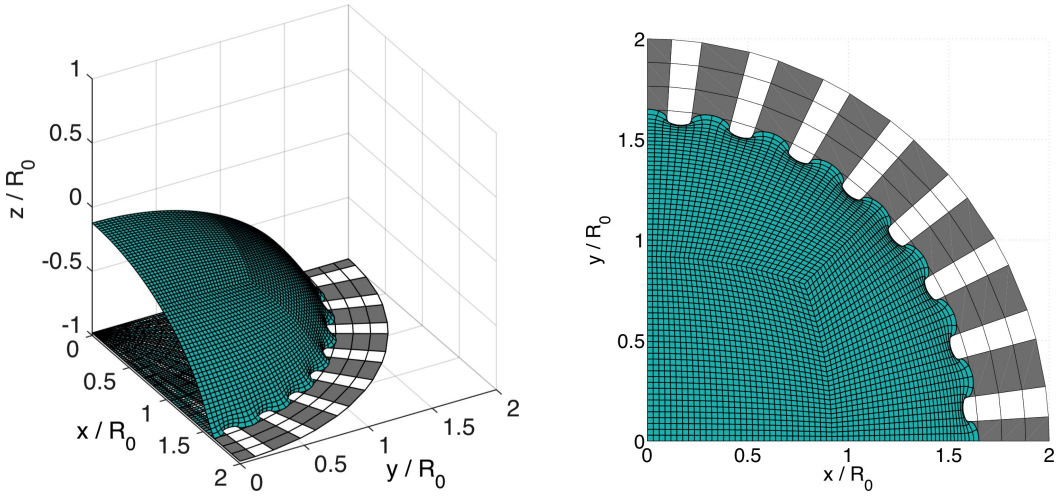

(b) $C = 2$

Figure 10: Deformation of the droplet at the final state of the wetting process for a dartboard-patterned chemical contamination $C = \{0.4, 2\}$ for $Bo = 1$, $\Phi_{\text{p}} = 5.625°$ and an initial contact angle $\theta_{\text{c}} = 105°$. The size of the dartboard-patterns changes by $\pm 1.3°$ during the wetting process. Left side: perspective view, right side: bottom (top right) and top (bottom right) view.

7 Summary and conclusion

The partial wetting of droplets on rigid, chemically heterogeneous/chemically contaminated substrates is investigated. A new computational contact-mechanical approach based on a Finite

Element Method (FEM) is utilized representing the droplet as a deforming liquid membrane under hydrostatic conditions. Numerical results are presented for Bond numbers $Bo \leq 5$ and chemically patterned (radially and/or circumferentially alternating) as well as locally chemically contaminated substrates. The numerical results presented for the shape of the droplet wetting a chemically heterogeneous substrate are in good agreement with analytical results in the absence of gravity ($Bo = 0$) and any contamination, and with numerical results in the absence of any contamination for ($0 < Bo \leq 5$), when transformed using a mapping based on the predicted change in the apparent contact angle. The mapping presented is derived via a perturbed force equilibrium analogy at the triple phase contact line predicting the contact angle change in the presence of a arbitrarily strong chemical contamination. The predicted change in the apparent contact angle is in agreement with the analytical theory by de Gennes (1985) for small perturbations and the modified Cassie's law (Cassie, 1948). The transformation allows for predicting the droplet's shape on chemically heterogeneous substrates for the case the entire triple phase contact line is affected by the contamination, provided the droplet shape is known for the case of a perfectly chemically homogeneous substrate. Thereby, the perturbed force equilibrium analogy allows for arbitrarily strong chemical contaminations extending the theory by de Gennes (1985). Additionally, the transformation may be applied to predict the droplet shape on a perfectly homogeneous substrate with contact angle $\theta_c = \theta_A$, provided the droplet shape is known for the wetting on another perfectly homogeneous substrate with $\theta_c = \theta_B \neq \theta_A$ for arbitrary Bond numbers.

The contact-mechanical approach is applied to a variety of chemical heterogeneities including axially patterned as well as radially patterned substrates, where no analytical theory is available anymore, demonstrating its robustness and flexibility. The results for the 3D droplet shape as well as for the wetting length, wetting area and droplet height is in agreement with results reported in literature.

Having demonstrated the capability of the newly developed numerical framework to accurately simulate the partial wetting process on rigid, chemically heterogeneous substrates in the present contribution, an extension is planned in a follow-up study towards the investigation of randomly chemically as well as spatially heterogeneous substrates. Furthermore, it is intended to extend the analytical mapping based on the perturbed force equilibrium analogy to the case of spatially heterogeneous substrates in analogy to de Gennes (1985).

Acknowledgements

The present work was funded by the German Science Foundation (DFG) research Grant no. GSC 111 through the Graduate School AICES. The authors would like to thank N. Pesheva and S. Iliev for helpful discussions and providing data for comparison in Fig. 9(e).

References

Adão, M. H., de Ruijter, M., Voué, M., and De Coninck, J. (1999). Droplet spreading on heterogeneous substrates using molecular dynamics. *Phys Rev E*, 59(1):746–750.

Bittoun, E. and Marmur, A. (2012). The Role of Multiscale Roughness in the Lotus Effect: Is It Essential for Super-Hydrophobicity? *Langmuir*, 28(39):13933–13942.

Bonn, D., Eggers, J., Indekeu, J., Meunier, J., and Rolley, E. (2009). Wetting and spreading. *Rev. Mod. Phys.*, 81(2):739–805.

Buehrle, J., Herminghaus, S., and Mugele, F. (2002). Impact of Line Tension on the Equilibrium Shape of Liquid Droplets on Patterned Substrates. *Langmuir*, 18(25):9771–9777.

Cassie, A. B. D. (1948). Contact angles. *Discussions of the Faraday Society*, 3:11.

Cassie, A. B. D. and Baxter, S. (1944). Wettability of porous surfaces. *Transactions of the Faraday Society*, 40:546.

de Gennes, P. G. (1985). Wetting: statics and dynamics. *Rev. Mod. Phys.*, 57(3):827–863.

Dupuis, A. and Yeomans, J. M. (2004). Lattice Boltzmann modelling of droplets on chemically heterogeneous surfaces. *Future Generation Computer Systems*, 20(6):993–1001.

Iliev, S. D. and Pesheva, N. C. (2003). Wetting Properties of Well-Structured Heterogeneous Substrates. *Langmuir*, 19(23):9923–9931.

Lenz, P. and Lipowsky, R. (1998). Morphological Transitions of Wetting Layers on Structured Surfaces. *Phys. Rev. Lett.*, 80(9):1920–1923.

Lipowsky, R., Lenz, P., and Swain, P. S. (1999). Wetting and dewetting of structured and imprinted surfaces. *Colloid. Surface A*, 161(1):3–22.

Lundgren, M., Allan, N. L., and Cosgrove, T. (2007). Modeling of Wetting: A Study of Nanowetting at Rough and Heterogeneous Surfaces. *Langmuir*, 23(3):1187–1194.

Quéré, D. (2008). Wetting and Roughness. *Ann. Rev. Mater. Res.*, 38(1):71–99.

Sauer, R. A. (2014). Stabilized finite element formulations for liquid membranes and their application to droplet contact. *Int. J. Num. Meth. Fluids*, 75(7):519–545.

Sauer, R. A., Duong, T. X., and Corbett, C. J. (2014). A computational formulation for constrained solid and liquid membranes considering isogeometric finite elements. *Comput. Meth. Appl. Mech. Eng.*, 271(C):48–68.

Savva, N. and Kalliadasis, S. (2009). Two-dimensional droplet spreading over topographical substrates. *Phys. Fluids*, 21(9):092102.

Savva, N., Kalliadasis, S., and Pavliotis, G. A. (2010). Two-Dimensional Droplet Spreading over Random Topographical Substrates. *Phys. Rev. Lett.*, 104(8):084501.

Schwartz, L. W. and Eley, R. R. (1997). Simulation of Droplet Motion on Low-Energy and Heterogeneous Surfaces. *J. Coll. Interf. Sci.*, 202(1):173–188.

Snoeijer, J. H. and Andreotti, B. (2013). Moving Contact Lines: Scales, Regimes, and Dynamical Transitions. *Ann. Rev. Fluid Mech.*, 45(1):269–292.

Vellingiri, R., Savva, N., and Kalliadasis, S. (2011). Droplet spreading on chemically heterogeneous substrates. *Physical Review E*, 84(3):036305.

Wenzel, R. N. (1936). Resistance of solid surfaces to wetting by water. *Industrial & Engineering Chemistry*, 28(8):988–994.

Woodward, J. T., Gwin, H., and Schwartz, D. K. (2000). Contact Angles on Surfaces with Mesoscopic Chemical Heterogeneity. *Langmuir*, 16(6):2957–2961.

Wriggers, P. (2006). *Computational Contact Mechanics*. Springer.

Wriggers, P. (2008). *Nonlinear Finite Element Methods*. Springer.

Yonemoto, Y. and Kunugi, T. (2014). Wettability model for various-sized droplets on solid surfaces. *Phys. Fluids*, 26:082110.